A Bayesian network for modelling blood glucose concentration and exercise in type 1 diabetes

Sean M. Ewings* and Sujit K. Sahu
Southampton Statistical Sciences Research Institute
University of Southampton, Southampton, SO17 1BJ, UK
Tel. (+44) 2380 595732 Email: sean.ewings@soton.ac.uk
John Joseph Valletta
Faculty of Engineering and the Environment
University of Southampton, UK
Christopher D. Byrne
Faculty of Medicine
University of Southampton, UK
Andrew J. Chipperfield
Faculty of Engineering and the Environment
University of Southampton, UK

December 5, 2013

Abstract

This article presents a new statistical approach to analysing the effects of everyday physical activity on blood glucose concentration in people with type 1 diabetes. A physiologically-based model of blood glucose dynamics is developed to cope with frequently-sampled data on food, insulin and habitual physical activity; the model is then converted to a Bayesian network to account for measurement error and variability in the physiological processes. A simulation study is conducted to determine the feasibility of using Markov chain Monte Carlo methods for simultaneous estimation of all model parameters and prediction of blood glucose concentration. Although there are problems with parameter identification in a minority of cases, most parameters can

be estimated without bias. Predictive performance is unaffected by parameter mis-specification and is insensitive to misleading prior distributions. This article highlights important practical and theoretical issues not previously addressed in the quest for an artificial pancreas as treatment for type 1 diabetes. The proposed methods represent a new paradigm for analysis of deterministic mathematical models of blood glucose concentration.

Keywords: Artificial pancreas; Bayesian network; exercise; free-living data; physical activity energy expenditure; type 1 diabetes.

1 Introduction

Understanding the effect of exercise on blood glucose concentration is crucial for people with type 1 diabetes, so that they are able to safely incorporate exercise into daily life. Understanding the effect of any physical activity experienced in everyday life can help improve treatment regimes, and hence reduce the risk of short- and long-term complications associated with diabetes [1] (see Section 1.1 for further background information on type 1 diabetes).

The effect of physical activity on internal physiological processes is rarely measurable, and certainly not in free-living conditions (defined here as without imposing constraints on an individual's ability to carry out their daily activities). Instead, mathematical models - i.e., systems of differential equations based on compartmental models - have been developed to describe blood glucose dynamics during exercise.[2–4] Such models play an important role in the ongoing development of an artificial pancreas[5] (described in the final paragraph of Section 1.1). However, these models are based on simplified exercise protocols and/or data from healthy volunteers that are not representative of everyday physical activity nor the diabetes population.

The first aim of this article is to assess the performance of a mathematical model of blood glucose dynamics: Section 2 describes the nature of free-living data collected during a Diabetes UK study,[6] which is used to assess both the model's ability to match profiles of blood glucose concentration and its handling of physical activity. We demonstrate a number of theoretical problems present in the model due to overlooking important properties of free-living data, and present a new physiologically-based model that is capable of handling such data.

The second aim of this article is to investigate the use of modern statistical methods for modelling blood glucose dynamics. We believe a stochastic model is a more accurate representation of the physiological processes of interest when compared with deterministic differential equations prevalent

elsewhere in blood glucose modelling; furthermore, we advocate individual-level parameter fitting to account for inter-person variability. Hence, Section 3 proposes a new stochastic approach for analysing our model (and therefore other models of blood glucose in the diabetes literature) where the differential equations are converted into a Bayesian network; we then propose Markov chain Monte Carlo (MCMC) methods for parameter estimation and prediction.

Performance of our new methods are tested using a simulation study, as presented in Section 4: we show that MCMC is able to estimate the majority of parameters without bias, and is able to predict blood glucose concentration under parameter misspecification and misleading prior information. Finally, Section 5 considers the application of our new model and approach to an individual from the Diabetes UK study, to test functionality in a real-world example.

In the wider context of diabetes research, understanding the nature of free-living data is necessary to understand the conditions in which an artificial pancreas must operate; thus, the practical and theoretical issues confronted in this article are vital in the work towards an artificial pancreas. This article also presents a departure from deterministic analysis of blood glucose, thereby acknowledging the complexity of glucose metabolism, and proposes methods applicable to a range of mathematical models of blood glucose.

1.1 Background

This section provides background information on type 1 diabetes and its treatment; it may be skipped by those familiar with this subject.

Type 1 diabetes (T1D) is a chronic metabolic disorder caused by the destruction of β-cells in the pancreas, resulting in the loss of endogenous insulin production; subsequently, blood glucose metabolism is disrupted, extreme hyperglycaemia (high blood glucose concentration) ensues, and, if untreated, coma and death can quickly follow.

Treatment of T1D is aimed at maintaining healthy blood glucose concentration ($\sim$75-120 mg/dl) with insulin injections. The common treatment regime involves a daily dose of long-lasting insulin and doses of rapid-acting insulin with meals; rapid-acting insulin doses are chosen according to the amount of carbohydrate consumed and any recent or imminent physical activity.

Good control of blood glucose concentration has been observed to slow, delay or prevent eye, kidney and nerve damage[1] and decrease incidence of cardiovascular events, such as stroke and heart attack,[7] by limiting the microvascular damage casued by hyperglycaemia; however, these benefits are

counteracted by increased incidence of hypoglycaemia (low blood glucose concentration), which can rapidly lead to seizures, unconsciousness and, if untreated, death. Determining the correct insulin dose is difficult, and T1D is associated with increased morbidity and mortality.[8]

Attempts to improve treatment regimes focus on optimising insulin delivery using an automated insulin delivery system (insulin pump); this approach requires a control algorithm to determine insulin dose based on frequent blood glucose measurements. Often, control algorithms require a description of blood glucose metabolism. The combination of blood glucose monitor, insulin pump and control algorithm is known as an artificial pancreas. Development of an artificial pancreas is ongoing,[9–12] and testing is currently limited to using simulated blood glucose profiles (from mathematical models of blood glucose metabolism) or small clinical trials.[13]

2 Data and methods

2.1 Data collection

Analysing the behaviour of blood glucose concentration (BGC) in free-living conditions requires frequently-sampled data to capture the rapid changes.[14] Capturing free-living data on internal physiological processes that affect BGC is not generally possible; instead, models of glucose metabolism may be used as a proxy, using easily-accessible measures, e.g., a model of the digestive process can use food intake to determine intestinal glucose absorption.

Diabetes UK recently funded a study to collect free-living data from volunteers with type 1 diabetes.[6] Volunteers wore two devices: a Guardian Real-Time Continuous Glucose Monitoring System (Medtronic MiniMed Inc., CA, USA) to frequently estimate BGC (based on measuring interstitial glucose concentration), and a SenseWear Pro2/3 armband (BodyMedia Inc., PA, USA) to estimate METs[15] (metabolic equivalent of task, a measure of energy expenditure). The nature of the devices ensured minimal impact on the individuals. Volunteers also recorded food intake (time, food type and estimated quantities) and insulin injections (time of injection, type of insulin and dose); glucose and insulin absorption profiles were subsequently estimated from these records using models of digestion[16] and insulin diffusion.[17] The study data therefore captures the major external disturbances to BGC.

During the study, BGC was recorded every five minutes, and physical activity data was recorded every minute and resampled every five minutes to correspond with the BGC readings; glucose and insulin absorption were estimated every five minutes, also to correspond with BGC readings. All

data was collected under free-living conditions.

An example of the nature of the data collected is given in Figure 1: 24-hour glucose and insulin absorption profiles from one volunteer (Subject A) in the study are shown in Figure 1 (i) and (ii), respectively, and Figure 1 (iii) shows Subject A's estimated METs over 24 hours. These data are used in the following section to assess the performance of a mathematical model of blood glucose dynamics, and are chosen as they are seen to reflect a relatively typical day: three meals (large peaks in glucose absorption) and snacks (smaller peaks), three injections of rapid-acting insulin (large peaks of insulin absorption) and one injection of long-lasting insulin, and fluctuating physical activity during the day.

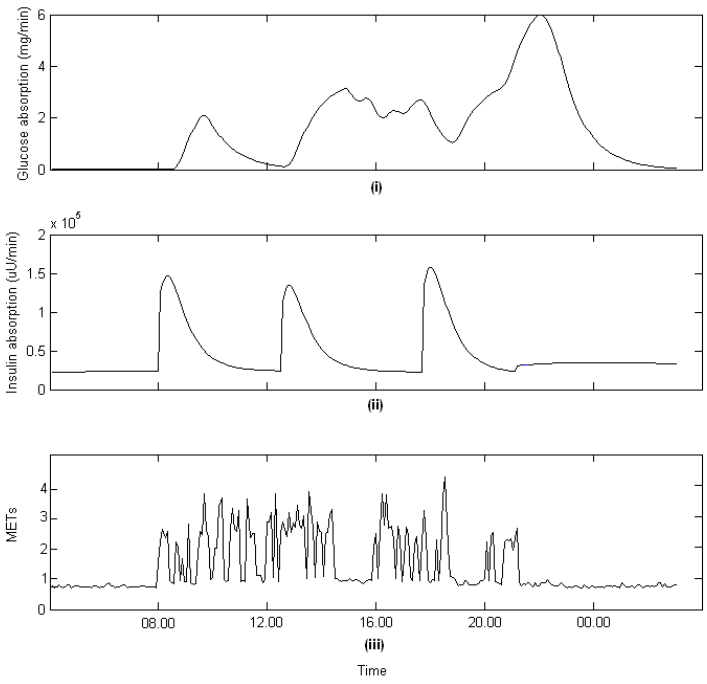

Figure 1: **(i)** Estimated glucose and **(ii)** insulin absorption (from digestion and insulin absorption models) and **(iii)** METs over 24 hours for Subject A.

The impact of food, insulin and physical activity on BGC may be assessed using mathematical models of blood glucose dynamics; in the following section we assess the ability of a recently-published mathematical model to describe the profile of blood glucose concentration using the study data.

2.2 Modelling blood glucose dynamics and exercise

Blood glucose dynamics are commonly described by compartmental models; landmark work was undertaken by Bergman and colleagues, who presented a "minimal model" of glucose-insulin dynamics[18,19] based on studies of blood glucose and insulin concentrations after glucose loads. The minimal model compartmentalises the body into the liver, periphery and blood according to their prominent roles in the body's response to a glucose load, and differential equations are used to describe blood glucose and insulin concentrations over time.

A number of extensions of the minimal model have been presented; of interest here is a model presented by Roy and Parker,[2] who extend the minimal model for use in type 1 diabetes. The model primarily focuses on extending the minimal model to account for exercise (it will be referred to as the exercise model from here on) and comprises nine differential equations (DEs), including six accounting for the effects of exercise, which are given in the appendix; the physiological basis of the equations and notation are summarised in Table 1.

Parameter estimates in the exercise model are based on data from healthy subjects performing simplified exercise protocols over short periods of time (<4 hours). It is not clear how the model would cope with free-living data such as that collected in the Diabetes UK study: we therefore begin by testing model performance using Subject A's data, chosen for the reasons previously stated in Section 2.1.

2.2.1 Modelling with free-living data

The model fails to accurately reflect BGC profiles, and returns non-viable results: e.g., Figure 2 shows that model-estimated blood glucose concentration drops below zero; blood insulin concentration is also found to drop below zero (not shown). The primary reason for poor model performance is the handling of physical activity: a key assumption of the exercise model is that activity returns to basal level after exercise, but data from the Diabetes UK study shows that physical activity does not return to basal level (1 METs) for extended periods during the day (as noticeable in Figure 1 (iii)); as a result, the roles of glycogenolysis and insulin clearance become disproportionately large.

We further believe that poor model performance is due to using data from healthy volunteers completing short-term exercise protocols for parameter estimation. These exercise regimes are unlikely to reflect everyday stimuli, and the response of BGC in healthy individuals is also unlikely to reflect that

Table 1: Summary of the differential equations in the exercise model.

Process	**Physiological description**
Blood glucose concentration (G)	Increased by food intake and hepatic glucose release; decreased by insulin-dependent and -indepedent hepatic and peripheral uptake
Blood insulin concentration (I)	Increased by insulin absorption after injection; decreased by insulin movement into active compartment
Active insulin (X)	Insulin active in promoting glucose metabolism; dependent on blood insulin concentration, and proportional to insulin concentration in a "remote" or active compartment (mimicking the process of insulin binding to cells before effecting its action)
Hepatic glucose release due to activity (H)	Activity stimulates the liver to release glucose from its stores into the blood
Peripheral glucose uptake due to activity (U)	Activity stimulates glucose transporters for blood glucose uptake in exercising muscle(s) to meet energy demands
Insulin clearance due to activity (Z)	Activity alters blood flow (increasing flow towards exercising muscle), increasing availability of insulin
Activity (E)	Introduces delay to measured activity to model the delay in physiological response to activity; measured by PVO_2^{max}, percentage of maximal oxygen uptake
Integrated activity	Accumulated activity over time
Decline in rate of glycogenolysis	Liver glucose resources are depleted during prolonged activity (as accounted for by integrated activity), resulting in attenuated glucose release

seen in people with type 1 diabetes. Due to the practical and theoretical flaws of the exercise model, a modified version of the model is presented in the following section.

2.3 Modified exercise model

The exercise model is modified to return physiologically-viable output: the rate of decline in glycogenolysis is removed (thus the model applies only to short- or medium-term, mild or moderate physical activity) as the current handling of activity is unsuitable; insulin clearance due to activity is removed (thus preventing negative blood insulin concentration), as this process may be modelling an effect not seen in type 1 diabetes;[20,21] and a term for renal

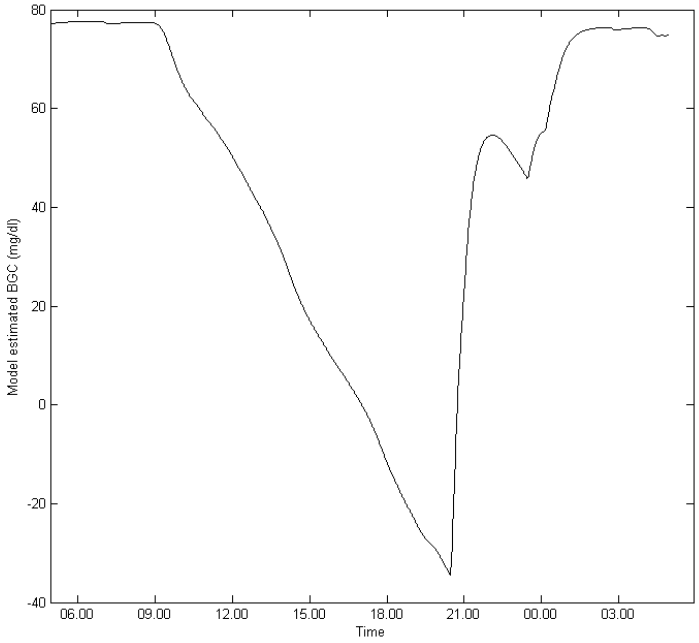

Figure 2: Estimated blood glucose concentration from the exercise model for Subject A.

clearance of blood glucose, as observed during periods of hyperglycaemia, is included in the blood glucose concentration DE (discussed below).

The modified physical activity model now comprises six DEs, which are discussed in the remainder of this section. Model parameters are described in Table 2 at the end of the section along with the model structure, in Figure 3, which describes the model's three subsystems (insulin subsystem, insulin-dependent glucose subsystem and insulin-independent glucose subsystem), the relationship between compartments and exchange of materials.

The insulin subsystem consists of two DEs. Blood insulin concentration (I; μU/ml) is modelled by

$$\frac{dI(t)}{d\mathrm{t}} = \dot{I}(t) = -p_1 I(t) + M_I(t)/V_I,$$

where p_1 is insulin clearance, $\mathrm{V_I}$ is the insulin distribution space, and $\mathrm{M_I}$ represents insulin absorption after injection. Active insulin (X; min^{-1}) refers to plasma insulin that has bound to insulin-sensitive cells, and is able to effect its action on blood glucose metabolism; this process is modelled by

$$\dot{X}(t) = -\,p_2 X(t) + p_3 I(t),$$

where p_2 is the rate of insulin degradation and p_3 is the rate of appearance of insulin in the active compartment from plasma.

The role of physical activity is accounted for in the insulin-independent glucose subsystem. As with the original exercise model, activity (E) is modelled with a delay to represent the delay between activity onset and physiological response:

$$\dot{E}(t) = -p_4 E(t) + p_5 M_E(t),$$

where $\mathrm{M_E}$ is the intensity of activity above basal level (8% $\mathrm{VO_2^{max}} \approx 1$METs). Physical activity encourages increased hepatic glucose release (H; mg/kg/min) and peripheral uptake (U; mg/kg/min); the effect of activity on each process is modelled by:

$$\dot{H}(t) = p_6 E(t) - p_7 H(t),$$
$$\dot{U}(t) = p_8 E(t) - p_9 U(t).$$

The blood glucose concentration (G; mg/dl) DE comprises the effect of basal hepatic balance and peripheral uptake, the roles of H, U, X, renal clearance (R), and glucose absorption after meals ($\mathrm{M_G}$):

$$\begin{aligned}\dot{G}(t) = &-p_{10}(G(t) - p_{11}) - X(t)G(t) \\ &+ (W/V_G)[H(t) - U(t) - R(t)] + M_G(t)/V_G,\end{aligned}$$

where p_{10} is insulin-independent glucose metabolism, p_{11} is basal BGC, W is the individual's weight, and V_G is the glucose distribution space. Renal clearance (R; mg/kg/min) depends on the threshold above which filtration occurs (r), filtration rate of the kidney (f) and blood glucose concentration: [22]

$$R = \mathrm{MA}[\max(0, f \cdot G - r)],$$

where MA represents a simple moving average of width 126mg/dl, which smooths the transition from no renal clearance to full clearance.

The modified exercise model represents a model of blood glucose dynamics that is able to handle free-living data. We believe parameter estimates should be based on free-living data, and fitted according to an individual's data rather than grouped data from clinical experiments. We also believe a stochastic model is a better representation of the physiological processes, as advocated elsewhere;[23] hence, we present a stochastic version of the modified exercise model in the following section, before considering parameter fitting methods.

Insulin subsystem

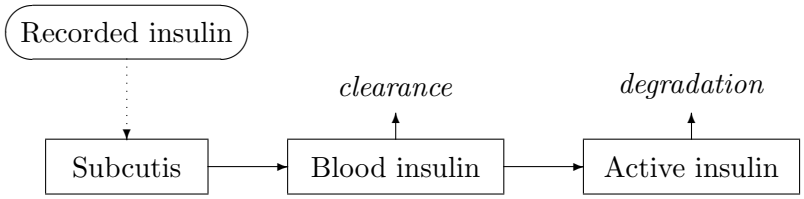

Insulin-dependent glucose subsystem

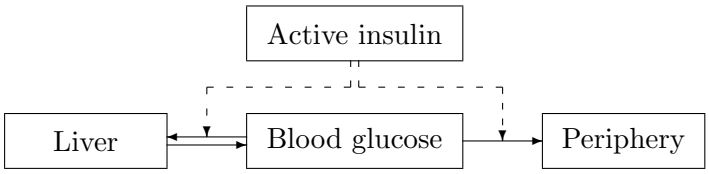

Insulin-independent glucose subsystem

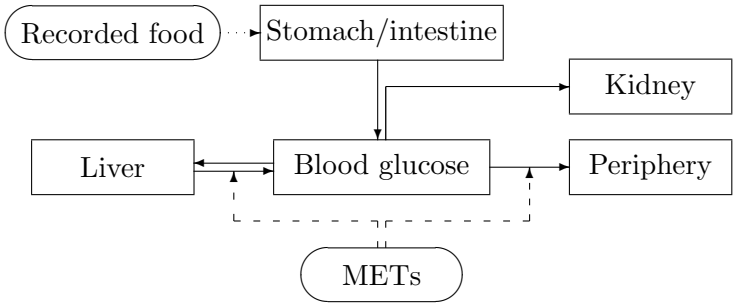

Figure 3: The new mathematical model of exercise and blood glucose concentration: ovals represent measured inputs and rectangular boxes represent compartments of the body; solid lines represent the exchange of insulin (in the insulin subsystem) or glucose; dashed lines represent where one process affects another; dotted lines represent where data from the Diabetes UK study is used as an input.

3 Bayesian network of blood glucose and exercise

The DEs of the modified exercise model are converted from deterministic form to a Bayesian network; the network is henceforth referred to as the stochastic exercise (SE) model. Bayesian methods are preferred in order to incorporate prior information on parameters and continually update belief as new data become available.

Using the blood glucose concentration DE as an example, the network is

Table 2: Parameters, processes and units of the modified exercise model.

Parameter	**Units**	**Parameter**	**Units**
p_1	min^{-1}	p_9	min^{-1}
p_2	min^{-1}	p_{10}	min^{-1}
p_3	$\text{ml}/\mu\text{U}/\text{min}^2$	p_{11}	mg/dl
p_4	min^{-1}	V_G	dl
p_5	min^{-1}	V_I	dl
p_6	mg/ml	W	kg
p_7	min^{-1}	r	mg/min
p_8	mg/ml	f	dl/min
Process		**Process**	
M_G	mg/min	M_I	μU/min
METs	ml/kg/min		

constructed as follows:

Assuming the processes are log-normally distributed,[23] convert the positive processes to the log scale with $g(t) = \ln[G(t)], \ldots, x(t) = \ln[X(t)]$, giving

$$\begin{aligned}\frac{\mathrm{d}g}{\mathrm{d}t} = \dot{g}(t) &= \dot{G}(t)/G(t) = \dot{G}(t)\exp[-g(t)] \\ &= -p_{10}\{1 - p_{11}\exp[-g(t)]\} - \exp[x(t)] + M_G(t)\exp[-g(t)]/V_G \\ &\quad + (W\exp[-g(t)]/V_G)\{\exp[h(t)] - \exp[u(t)] - R(t)\}.\end{aligned}$$

The DE is appended with a stochastic term represented by Brownian motion, $w_g(t)$, with associated precision, τ_g. By convention, such a stochastic DE is written as:

$$\begin{aligned}\mathrm{d}g(t) = \big\{ &- p_{10}\{1 - p_{11}\exp[-g(t)]\} - \exp[x(t)] \\ &+ (W\exp[-g(t)]/V_G)\{\exp[h(t)] - \exp[u(t)] - R(t)\} \\ &+ M_G(t)\exp[-g(t)]/V_G\big\}\mathrm{d}t + (\tau_g^{-1/2})\mathrm{d}w_g(t).\end{aligned}$$

This is converted to an integral equation by integrating over a small time frame, t to $t + \delta$, for small $\delta > 0$, assumed constant here:

$$\begin{aligned}g(t+\delta) - g(t) = \int_t^{t+\delta} \Big\{ &- p_{10}\{1 - p_{11}\exp[-g(t)]\} - \exp[x(t)] \\ &+ \{W\exp[-g(t)]/V_G\}\{\exp[h(t)] - \exp[u(t)] - R(t)\} \\ &+ M_G(t)\exp[-g(t)]/V_G\Big\}\mathrm{d}t + \epsilon_g(t),\end{aligned}$$

where $\epsilon_g(t) = \tau_g^{-1/2}[w_g(t+\delta) - w_g(t)]$. The integral is approximated by the product of the width and the integrand evaluated at the lower limit. The model is now concerned with discrete rather than continuous time, hence a change in notation of the form $g(t) = g_t$ and $\epsilon_g(t) = \epsilon_{g,t}$. The change in blood glucose concentration over the time span δ is now given by

$$\begin{aligned} g_{t+1} - g_t = \delta\{&-p_{10}[1 - p_{11}\exp(-g_t)] - \exp(x_t) \\ &+ [W\exp(-g_t)/V_G][\exp(h_t) - \exp(u_t) - R_t] \\ &+ M_{G,t}\exp(-g_t)/V_G\} + \epsilon_{g,t+1}. \end{aligned}$$

Standard results for Brownian motion[24] gives $\epsilon_{g,t+1} \sim N(0, \delta\tau_g^{-1})$. Setting

$$\begin{aligned} f_{g,t+1} = g_t + \delta\{&-p_{10}[1 - p_{11}\exp(-g_t)] - \exp(x_t) \\ &+ [W\exp(-g_t)/V_G][\exp(h_t) - \exp(u_t) \\ &- R_t] + M_{G,t}\exp(-g_t)/V_G\} \end{aligned} \tag{1}$$

gives $g_{t+1} = f_{g,t+1} + \epsilon_{g,t+1}$, and hence

$$(g_{t+1}|g_t, x_t, h_t, u_t) \sim N(f_{g,t+1}, \delta\tau_g^{-1}), \tag{2}$$

ignoring for convenience the dependence of latent processes on the equation parameters. Thus, BGC is now represented by a series of distributions at discrete points in time. Following the same procedure for each DE in Section 2.3 gives

$$\begin{aligned} (i_{t+1}|i_t) &\sim N(f_{i,t+1}, \delta\tau_i^{-1}) \\ (x_{t+1}|x_t, i_t) &\sim N(f_{x,t+1}, \delta\tau_x^{-1}) \\ (e_{t+1}|e_t) &\sim N(f_{e,t+1}, \delta\tau_e^{-1}) \\ (h_{t+1}|h_t, e_t) &\sim N(f_{h,t+1}, \delta\tau_h^{-1}) \\ (u_{t+1}|u_t, e_t) &\sim N(f_{u,t+1}, \delta\tau_u^{-1}), \end{aligned} \tag{3}$$

where

$$\begin{aligned} f_{i,t+1} &= i_t + \delta[-p_1 + M_{I,t}\exp(-i_t)/V_I] \\ f_{x,t+1} &= x_t + \delta[-p_2 + p_3\exp(-x_t)\exp(i_t)] \\ f_{e,t+1} &= e_t + \delta[-p_4 + p_5 M_{E,t}\exp(-e_t)] \\ f_{h,t+1} &= h_t + \delta[p_6\exp e_t\exp(-h_t) - p_7] \\ f_{u,t+1} &= u_t + \delta[p_8\exp e_t\exp(-u_t) - p_9]. \end{aligned} \tag{4}$$

Uncertainty is also assumed present in BGC observations: on the log scale, observed BGC (g_t^*) is assumed to have measurement error modelled by white noise, with expectation equal to the underlying latent process,

$$g_t^*|(g_t, \tau_{g^*}) \sim N(g_t, \tau_{g^*}^{-1}). \tag{5}$$

BGC observations and the six processes of the model may be represented by a directed acyclic graph (Figure 4), which shows the conditional relationships between processes and observations.

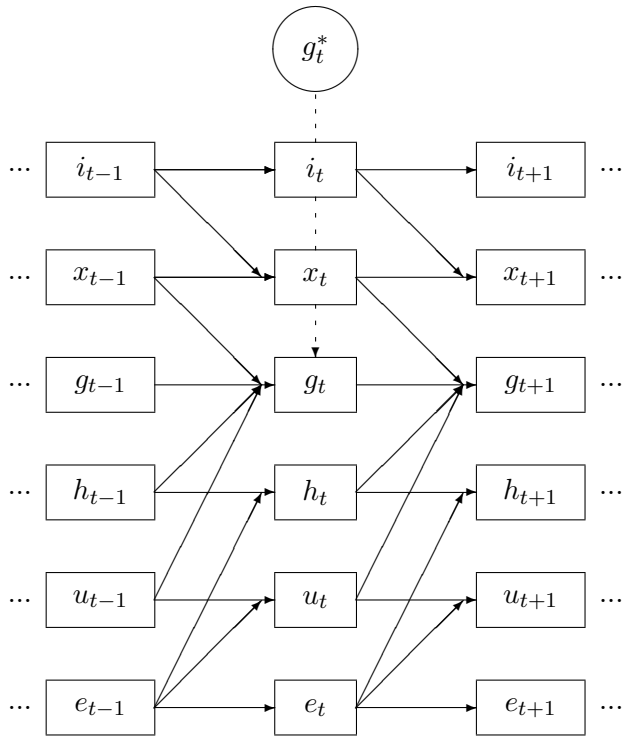

Figure 4: Directed acyclic graph of the modified exercise model.

The Bayesian approach is completed by modelling uncertainty in parameters using prior distributions: the natural logarithm of the positive equation parameters, $\{p_1, \ldots, p_{11}, V_G, V_I\}$, are assumed to have a normal prior distribution, e.g.,

$$\ln(p_1) \sim N(\mu_{p_1}, \tau_{p_1}^{-1}), \tag{6}$$

and the precisions, $\{\tau_{g^*}, \tau_g, \ldots, \tau_u\}$, are assumed to have a conditionally conjugate gamma prior distribution[1], e.g.,

$$\tau_g \sim \text{Gamma}(\alpha_{\tau_g}, \beta_{\tau_g}). \tag{7}$$

Analysis and inference reagarding the SE model is based on the posterior distribution, as determined by Bayes' Theorem.

[1]The gamma parameterisation used here and throughout specifies that if $X \sim G(\alpha, \beta)$ then $p(X; \alpha, \beta) \propto X^{\alpha-1} \exp(-X\beta)$.

3.1 Posterior distribution of the SE model

For convenience, the equation parameters, precisions and latent processes are split into three groups:

$$\begin{aligned}\Omega_1 =&\{p_1, p_2, p_3, p_4, p_5, p_6, p_7, p_8, p_9, p_{10}, p_{11}, V_G, V_I\},\\ \Omega_2 =&\{\tau_g, \tau_i, \tau_x, \tau_h, \tau_u, \tau_e, \tau_{g^*}\},\\ \Phi =&\{\boldsymbol{g}, \boldsymbol{i}, \boldsymbol{x}, \boldsymbol{h}, \boldsymbol{u}, \boldsymbol{e}\},\end{aligned}$$

with the full collection denoted by $\boldsymbol{\theta} = \{\Omega_1, \Omega_2, \Phi\}$. By Bayes' Theorem, the full, joint posterior distribution of all unobserved quantities is given by

$$\begin{aligned}p(\boldsymbol{\theta}|\boldsymbol{g}^*) &\propto p(\boldsymbol{g}^*|\boldsymbol{\theta})p(\boldsymbol{\theta})\\ &\propto p(\boldsymbol{g}^*|\boldsymbol{\theta})p(\Phi|\Omega_1, \Omega_2)p(\Omega_1)p(\Omega_2),\end{aligned} \tag{8}$$

where $\boldsymbol{g^*} = \{g_1^*, \ldots, g_T^*\}$ represents the set of BGC observations. The first part of the likelihood, $p(\boldsymbol{g}^*|\boldsymbol{\theta})$, is determined by (5):

$$p(\boldsymbol{g}^*|\boldsymbol{\theta}) = \prod_{t=1}^{T} p(g_t^*|g_t, \tau_{g^*}) \propto (\tau_{g^*})^{T/2} \exp[(-\tau_{g^*}/2) \sum_{t=1}^{T} (g_t^* - g_t)^2].$$

The second part of the likelihood consists of the joint distribution of the latent processes, given by:

$$p(\Phi|\Omega_1, \Omega_2) = \prod_{t=1}^{T} p(g_t|\cdot)p(i_t|\cdot)p(x_t|\cdot)p(e_t|\cdot)p(h_t|\cdot)p(u_t|\cdot)$$

where, e.g., $p(g_t|\cdot)$ implies the conditional distribution of g_t given all other parameters in Ω_1, Ω_2 and Φ. This joint distribution is determined by equations (1)–(4):

$$\begin{aligned}p(\Phi|\Omega_1, \Omega_2) \propto&(\tau_g\tau_i\tau_x\tau_e\tau_h\tau_u\tau_y\tau_k)^{T/2} \exp\Big\{ -\frac{1}{2\delta} \sum_{t=1}^{T} \big[\tau_g(g_t - f_{g,t})^2\\ &+\tau_i(i_t - f_{i,t})^2 + \tau_x(x_t - f_{x,t})^2 + \tau_e(e_t - f_{e,t})^2\\ &+\tau_h(h_t - f_{h,t})^2 + \tau_u(u_t - f_{u,t})^2\big]\Big\}.\end{aligned}$$

The final terms in the full posterior distribution are determined by (6) and (7), where

$$\begin{aligned}p(\Omega_1) = &p(p_1)p(p_2)p(p_3)p(p_4)p(p_5)p(p_6)p(p_7)p(p_8)p(p_9)p(p_{10})\\ &\times p(p_{11})p(V_G)p(V_I)\end{aligned}$$

and

$$p(\Omega_2) = p(\tau_{g^*})p(\tau_g)p(\tau_i)p(\tau_x)p(\tau_e)p(\tau_h)p(\tau_u),$$

assuming independence of the parameters and precisions.

The SE model represents a highly complex, nonlinear system. We therefore advocate the use of Markov chain Monte Carlo (MCMC) methods[25] as a tool for parameter fitting and prediction of BGC. The suitability of MCMC methods may be tested using a simulation study, where fixed parameter values are used to generate a BGC profile and MCMC estimates are derived for the (known) parameters.

4 Simulation study

Parameters in Ω_1 are fixed to previously-reported values[2] (the value of parameter p_3 was altered as it led to an unstable blood insulin time series), and the precisions in Ω_2 are also fixed at arbitrary values; all values are given in Table 3. Glucose and insulin absorption from 24 hours of a volunteer's (Subject A) records are used as the inputs M_G and M_I, respectively, and the same day's physical activity (METs) measurements are used as the input M_E; these inputs are as presented in Figure 1 previously.

Table 3: Parameter values used to generate BGC time series for simulation study.

Parameter	**Value**	**Parameter**	**Value**
p_1	0.142	W	70
p_2	0.05	V_G	117
p_3	0.00028	V_I	1760
p_4	0.8	τ_g	5
p_5	0.8	τ_i	5
p_6	0.00158	τ_x	5
p_7	0.056	τ_h	5
p_8	0.00195	τ_u	5
p_9	0.0485	τ_{g^*}	5
p_{10}	0.035		
p_{11}	80		

The conditional distributions presented in equations (2) and (3) are used to simulate values of the latent processes, Φ, every five minutes over a 24-hour period (288 time points). BGC "observations" are then simulated using equation (5); the simulated data are presented in Figure 6 (along with MCMC output, as discussed later). Given this series of observations, MCMC methods are used to estimate the parameters in Ω_1 and Ω_2.

4.1 Preliminary analysis

Given the complexity of the model (with regard to the number of processes and parameters), the computational burden is large (on an Intel Core 2 Duo CPU with 1.95GB of RAM, 1000 iterations of a chain takes approximately 20 minutes); to reduce this burden, the process E and associated parameters, p_4 and p_5, are treated as known. The process E describes the body's delayed response to physical activity, i.e., the delayed increase in heart rate and oxygen uptake, and introduces a lag on the impact of activity on other processes; its intended behaviour is therefore well understood, and it is dependent only on armband measurements. The parameters p_4 and p_5 are fixed to 0.8 and the DE for E is solved to coincide with BGC measurements. Solutions at each time point are treated as known in the rest of the model.

The remaining parameters in Φ and Ω_1 are updated using the single-component Metropolis-Hastings algorithm, as their conditional posterior distributions are not of standard form. The normal distribution is chosen as the proposal density for each parameter, with the mean determined by the current state of the chain, i.e., for parameter θ_i, the proposal distribution at iteration j is $N(\theta_i^{(j-1)}, \lambda_i)$, for given variance, λ_i. Parameters in Ω_2 are updated using Gibbs sampling, as the conditional posterior distributions are from the gamma family.

The means of the prior distributions for parameters in Ω_1 are chosen to be the values previously presented (Table 3) and the variances are chosen to be relatively large, e.g.,

$$\alpha_1 = \ln(p_1) \sim N(\ln(0.142), 1).$$

The prior distributions of parameters in Ω_2 are given by

$$\tau_g \sim \text{Gamma}(2, 1),$$

a weakly-informative prior distribution.

Starting values for the equation parameters and precisions are chosen to be the means of their respective priors, e.g., $\alpha_1^{(0)} = \ln(0.142)$ and $\tau_g^{(0)} = 2$. The latent processes are given arbitrary starting values across all time points: $\forall t$, $g_t = \ln(p_{11}) = \ln(80)$, $i_t = -5$, $x_t = -5$, $h_t = -5$, and $u_t = -5$.

A series of pilot studies, using chains of length 5 000–10 000, were run to determine suitable values of the λ_i; these values were repeatedly tuned in order to return acceptance rates of between 0.15 and 0.5 for each parameter in Φ and Ω_1. It was found that the high correlation between successive time points in the latent processes led to occasional poor mixing; however, blocking the processes in Φ led to very slow convergence in this case and so was not pursued.

The pilot studies highlight the difficulty of estimating all parameters in Φ and Ω_1: in particular, a number of parameter estimates are highly negative, suggesting the parameters are zero on the original scale; Figure 5 shows the trace plot for p_3 from a chain of length 50 000 with burn-in 20 000. Six parameters (p_3, p_7, p_9, p_{11}, V_G and V_I) displayed such behaviour and are omitted from the MCMC estimation procedure (and hence fixed for the remainder of the simulation study). For the remaining parameters ($\Omega_1^*=\{p_1, p_2, p_6, p_8, p_{10}\}$), results using over-dispersed starting values (not shown) suggested a burn-in of 5 000 is acceptable for estimation. Chains of length 10 000 (including burn-in) suggested posterior estimation of BGC agrees well with simulated BGC (Figure 6).

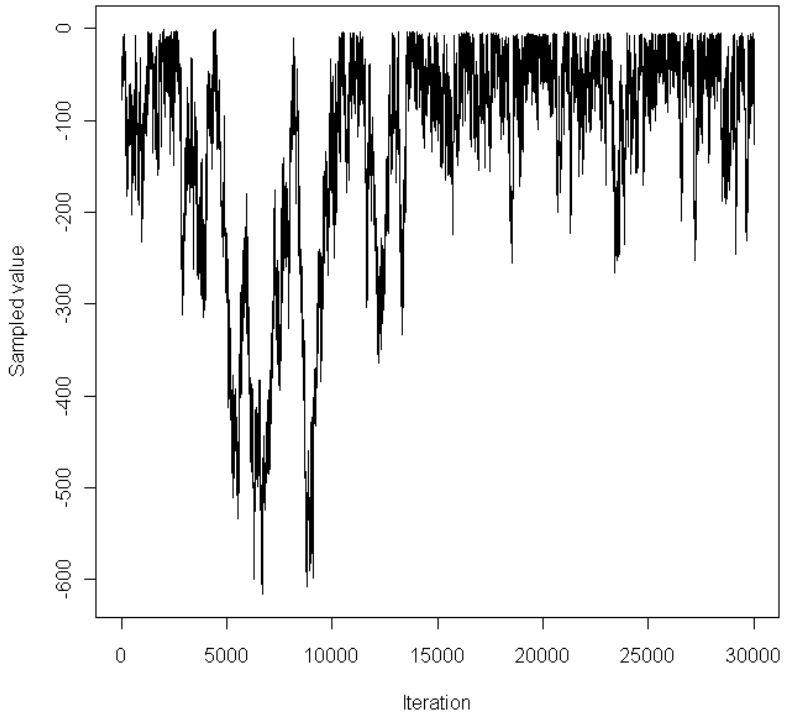

Figure 5: MCMC trace plot for p_3 from a long chain.

4.2 Results

Fifty data sets are simulated, and a Markov chain of size 10 000 (with burn-in of 5 000) is used to estimate parameters in Ω_1 and Ω_2 for each set. Corre-

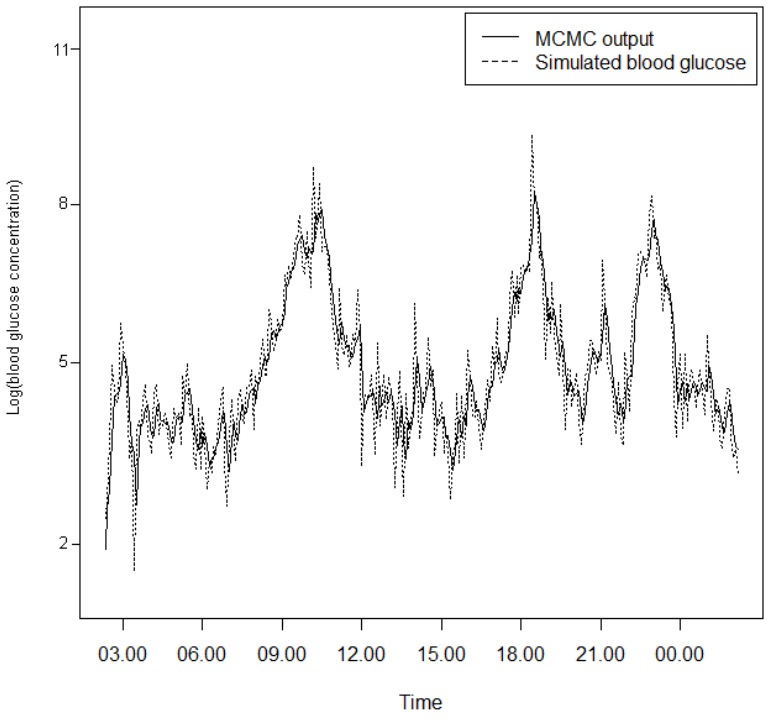

Figure 6: Simulated BGC and MCMC output.

sponding 95% credible intervals are found by determining the 2.5^{th} and 97.5^{th} precentiles according to ascending order of the sampled values. MCMC performance was assessed by comparison of credible intervals from all chains against the true parameter value (expressed as a percentage of intervals containing the true value).

Figures 7-9 show means and 95% credible intervals for parameters p_1, p_8 and p_{10}, respectively, ordered by mean. Figure 7 shows 68% of credible intervals contain p_1, below the ideal of 95%; this may be due to an inadequate burn-in period, where non-convergence of the chain has led to poor parameter estimation. However, the large computational burden (50 chains of 10 000 iterations required seven days to run) meant a larger simulation study could not be conducted to thoroughly investigate this. Results similar to those of p_1 were seen for parameters p_2 and p_6. Figure 8 shows consistent underestimation of p_8; this implies there may be issues with parameter identification, where different values of p_8 return the same distribution of observations. In contrast, Figure 9 shows better performance for p_{10}, with

the majority (90%) of credible intervals containing the value of p_{10} used to generate the simulated BGC.

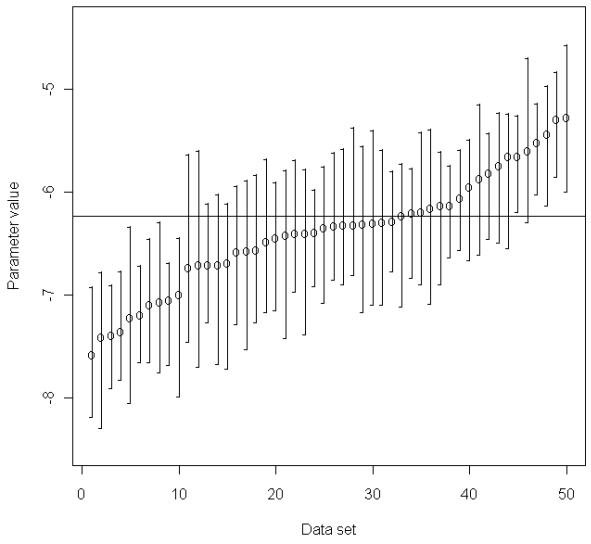

Figure 7: Means and 95% credible intervals for p_1 from each Markov chain in the simulation study; the horizontal line represents the value of p_1 used to generate the simulations.

Figures 10 and 11 show means and credible intervals for precisions τ_i and τ_{g^*}, respectively, ordered by mean. The results for τ_i (Figure 10) are typical of those seen for τ_x, τ_h and τ_u, with all credible intervals containing the value of the respective τ but a tendency for overestimation. The results for τ_{g^*} (Figure 11) show all credible intervals contain the simulation value, without obvious bias, and is similar to the results seen for τ_g.

4.3 Model Verification

MCMC methods may be further assessed by monitoring performance in the predictive space; this was achieved by removing a selection of BGC measurements (to be used as verification values) according to a number of scenarios:

- **scenario A** 25 randomly-selected measurements;
- **scenario B** one-hour block during early morning (when asleep);
- **scenario C** one-hour block after breakfast, and three-hour block after an evening meal and into the night.

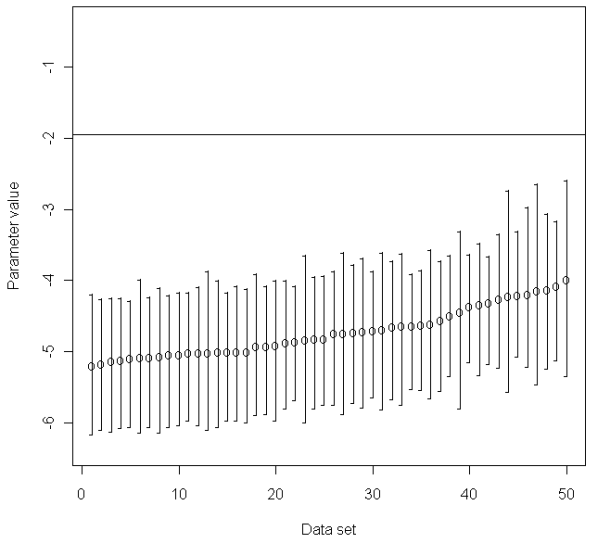

Figure 8: Means and 95% credible intervals for p_8 from each Markov chain in the simulation study; the horizontal line represents the value of p_8 used to generate the simulations.

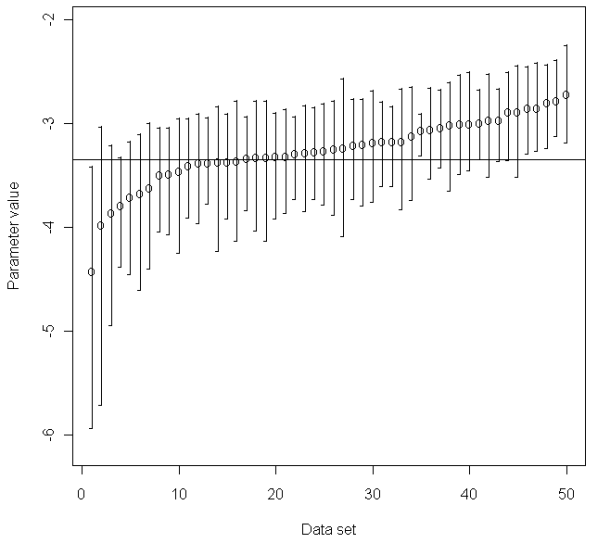

Figure 9: Means and 95% credible intervals for p_{10} from each Markov chain in the simulation study; the horizontal line represents the value of p_{10} used to generate the simulations.

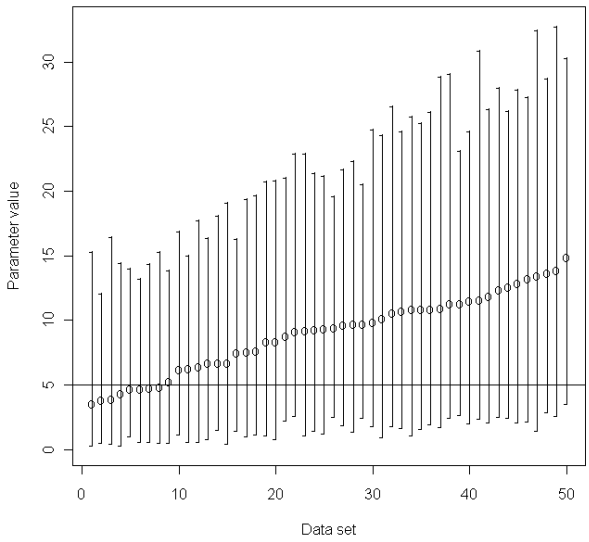

Figure 10: Means and 95% credible intervals for τ_i from each Markov chain in the simulation study; the horizontal line represents the value of τ_i used to generate the simulations.

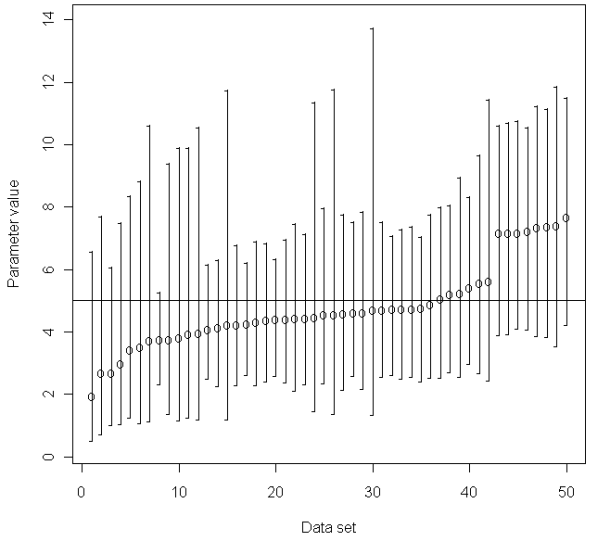

Figure 11: Means and 95% credible intervals for τ_{g^*} from each Markov chain in the simulation study; the horizontal line represents the value of τ_{g^*} used to generate the simulations.

The MCMC methods used in the previous section are extended to sample from the distribution of BGC measurements (equation 5); Gibbs sampling is used as the conditional posterior distribution of BGC measurements is a normal distribution. Chains of size 20 000, including burn-in of 5 000, are run to determine the ability of MCMC to predict measured BGC. Starting values of the missing observations are chosen to be $\ln(p_{11}) = \ln(80)$.

4.3.1 Results

For each scenario, MCMC sample means and 95% credible intervals are calculated for each missing BGC measurement. Figure 12 suggests good predictive performance under scenario 1 (random missing measurements), with the credible intervals all containing the true value, and no obvious prediction bias. Figure 13 shows the results for scenario 2, with the credible intervals again containing the simulated BGC entirely. However, the intervals are so wide as to be of limited use in practical terms; e.g., an interval of (1,8) is equivalent to BGC in the range $\sim$(3,2980)mg/dl, which spans much of the hypo- and hyperglycaemic range. The width of the confidence intervals is due to the (arbitrarily chosen) values of the precisions; different choices of these precisions results in different confidence intervals.

Figures 14 and 15 show the results for scenario 3, split into blocks of verification values; these show that the credible intervals contain the simulated BGC almost entirely (one interval does not). The MCMC sample means do not appear to pick up the fluctuating nature of the simulated BGC.

4.4 Robustness

Predictive performance may also be assessed by testing robustness to specification of prior distributions or misspecification of parameters. Predictive performance is assessed over 25 randomly-selected BGC simulated values across a number of arbitrarily-determined scenarios, involving either (misleading) informative prior distributions, parameter misspecification, or a combination:

- **scenario 1** (baseline scenario) all fixed parameters kept at simulation values, prior distributions as specified in Section 4.1. The remaining scenarios are as scenario 1 except where specified;
- **scenario 2** overestimation of p_{11} (simulation value of 80mg/dl; fixed value of 90mg/dl);
- **scenario 3** ten-fold overestimation of p_7 (0.056; 0.56) and underestimation of V_I (176dl; 150dl);

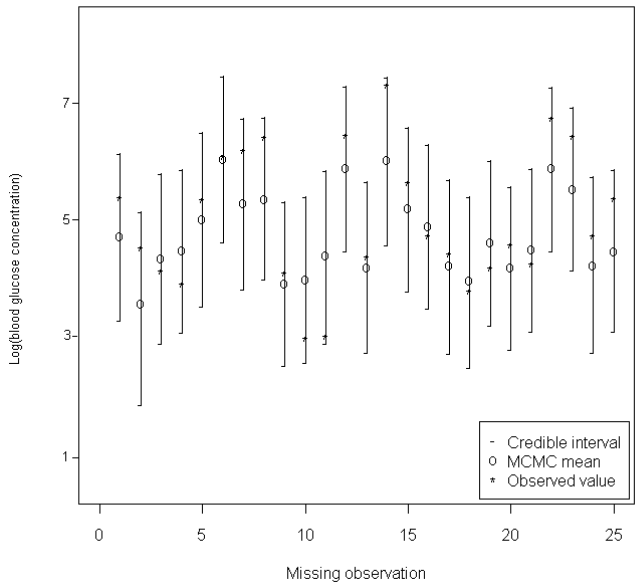

Figure 12: Means and 95% credible intervals for each missing observation under scenario A.

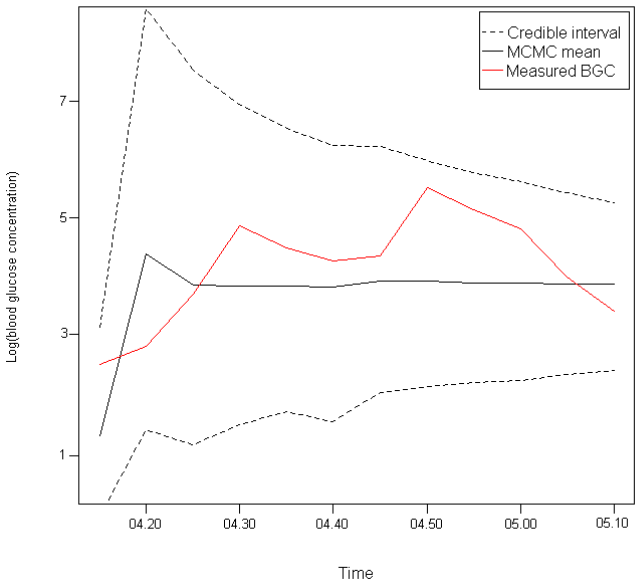

Figure 13: Means and 95% credible intervals for each missing observation under scenario B.

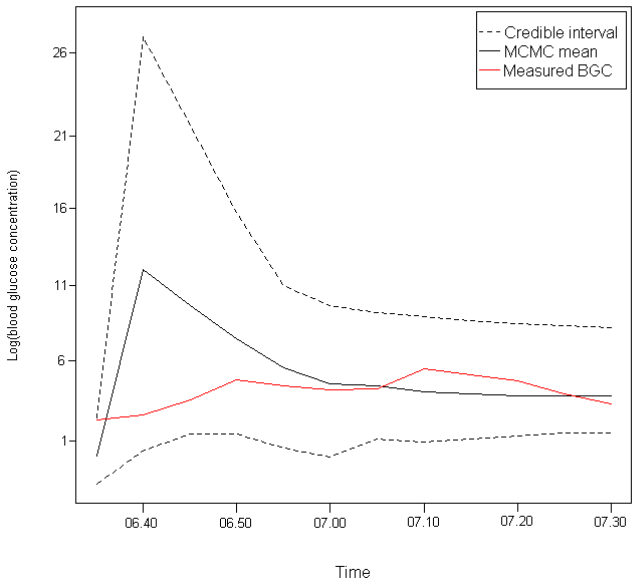

Figure 14: Means and 95% credible intervals for each missing observation under scenario C (first block).

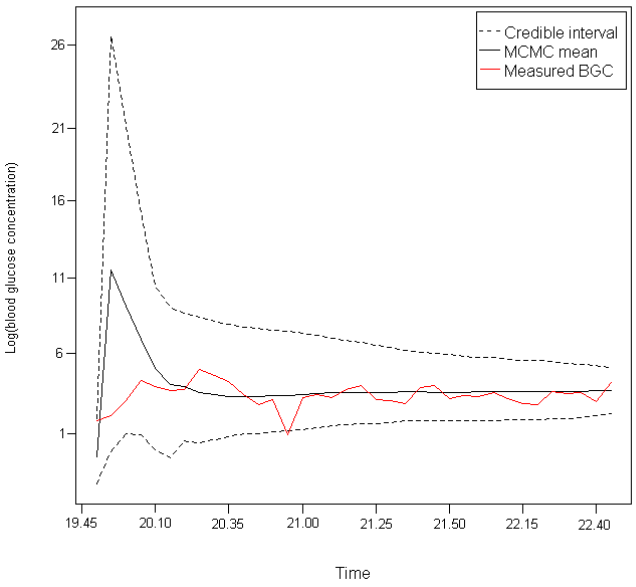

Figure 15: Means and 95% credible intervals for each missing observation under scenario C (second block).

- **scenario 4** ten-fold underestimation of p_9 (0.0485; 0.00485), prior distribution for p_8 given by $N(1, 0.1)$;
- **scenario 5** all fixed parameters kept at simulation values, with prior distributions $\tau_g \sim \text{Gamma}(10, 10)$ and $\tau_i \sim \text{Gamma}(0.1, 0.1)$;
- **scenario 6** prior distribution $p_{10} \sim N(0.35, 3)$;
- **scenario 7** all equation parameter prior distributions set to $N(5, 0.01)$, 100-fold overestimation of p_3 (0.000028; 0.0028), ten-fold underestimation of p_7 (0.056; 0.0056) and overestimation of V_G (117dl; 140dl).

The continuous ranked probability score (CRPS)[26] is used to compare the cumulative distribution of the MCMC samples in each scenario to the true value, thereby providing a comparable measure of model performance in each scenario.

4.4.1 Results

Estimated CRPS for each of the scenarios is given in Table 4. CRPS is relatively consistent across the scenarios, suggesting the model is robust to misspecification of parameters and/or different specification of prior distributions. In particular, all scenarios performed at a similar level to scenario 1, suggesting, at worst, only a minor loss of predictive performance compared to the standard set-up.

Table 4: CRPS values under scenarios given in Section 4.4.

Scenario	**CRPS**
1	0.395
2	0.397
3	0.410
4	0.393
5	0.393
6	0.400
7	0.412

Having established the use of our new methods in a simulation study, we now turn attention to a real-world example.

5 Case Study

MCMC is used to estimate parameters in Ω_1^*, Ω_2 and Φ for Subject A. All prior distributions and starting points are as in the simulation study (Section 4.1). A chain of length 50 000 with burn-in of 20 000 is used to determine parameter estimates.

5.1 Results

Errors between estimated BGC and observed BGC are given in Figure 16; the plot shows close agreement of estimated and observed BGC. Estimates and associated credible intervals of parameters in Ω_1^* and Ω_2 are given in Table 5; the results suggest some deviation from parameter estimates derived in the Roy and Parker model,[2] indicating there may be significant and potentially important differences between parameter values across individuals.

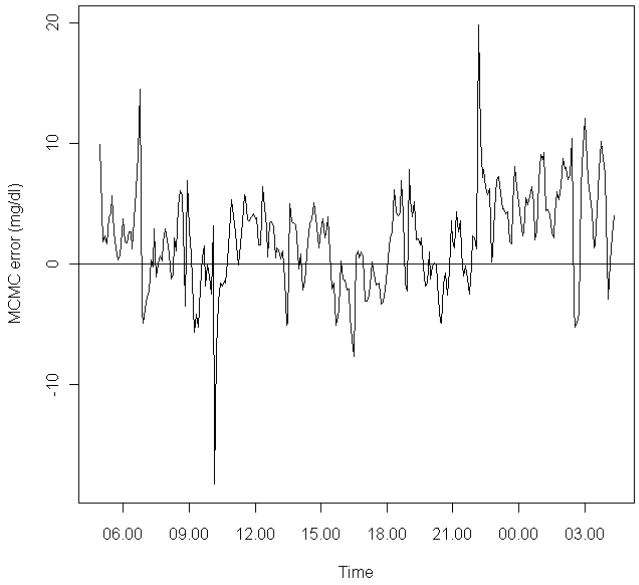

Figure 16: Errors between MCMC-estimated BGC and observed BGC.

The estimated profile of plasma insulin concentration (I) is given alongside estimated insulin absorption in Figure 17: peaks in plasma insulin coincide with insulin injections, suggesting the model is behaving as would be expected with regard to the insulin subsystem; similar results are seen for

Table 5: MCMC parameter estimates and associated 95 % credible intervals (CI) for Subject A.

Parameter	**MCMC estimate**	**95% CI**
p_1	-1.47	(-1.97, -0.98)
p_2	-1.65	(-2.28, -1.18)
p_6	-6.75	(-7.49, -5.31)
p_8	-8.24	(-9.44, -6.51)
p_{10}	-3.52	(-5.27, -2.43)
τ_{g^*}	3.78	(1.88, 5.80)
τ_g	3.31	(1.63, 5.12)
τ_i	7.29	(3.02, 14.13)
τ_x	12.32	(1.73, 31.96)
τ_h	10.21	(1.18, 25.23)
τ_u	9.86	(1.10, 24.34)

active insulin (X), with a slight shift in time (to the right) accounting for the process by which plasma insulin binds to insulin-sensitive cells.

Figure 18 shows increased peripheral glucose uptake (U) with increased physical activity, suggesting the model is again behaving as expected. However, there is evidence of instability when U becomes too negative (similar results are seen for H); this may be due to model instability when U$\rightarrow 0 \Rightarrow u = \ln(U) \rightarrow -\infty$.

Mixing is generally excellent across all time points for the processes G, I and X; Figure 19 shows a set of trace plots (arbitrarily-selected) for these processes. Mixing is more variable for processes H and U: Figure 20 shows good mixing at early time points which becomes less satisfactory at later time points. Mixing is excellent for the precisions in Ω_2; Figure 21 shows the trace plots for τ_g and τ_x, which are typical of the other precisions. For the remaining parameters, in Ω_1^*, mixing is less satisfactory; trace plots suggest non-convergence - as exemplified by the trace plot of p_2 (Figure 22 (i)) - except in the case of p_{10}, which has excellent mixing (Figure 22 (ii)).

6 Discussion

This article highlighted a number of practical and theoretical issues relating to the combination of free-living data and mathematical models of blood glucose, which represents an important step towards the development of an artificial pancreas.

We have demonstrated major differences between free-living activity and simplified exercise protocols in a clinical environment, and how this can vi-

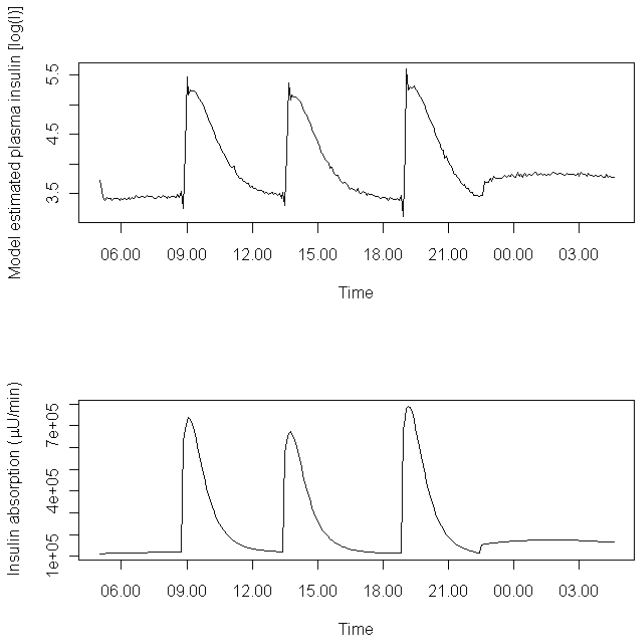

Figure 17: Model-estimated plasma insulin concentration (top) and insulin absorption after injection (from insulin absorption model; bottom) for Subject A.

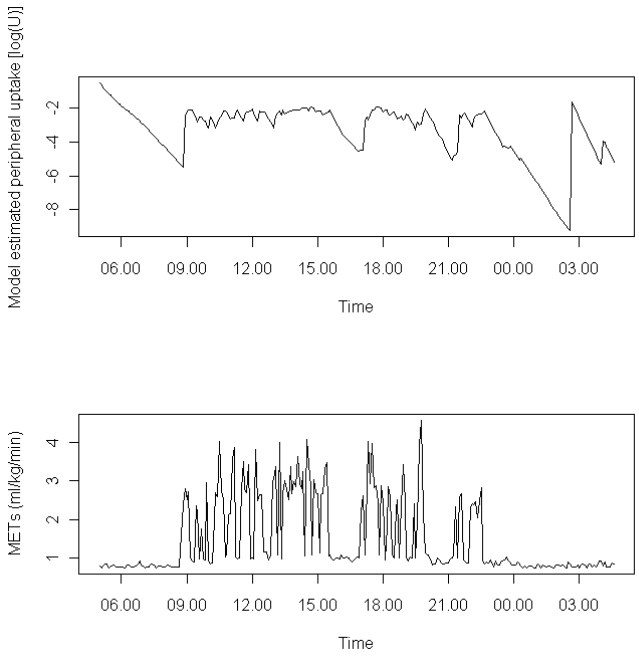

Figure 18: Model-estimated peripheral glucose uptake due to physical activity (top) and METs (bottom) for Subject A.

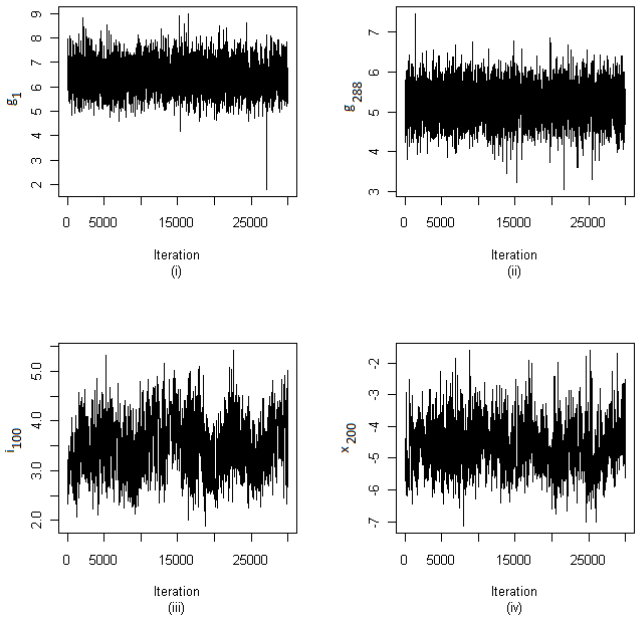

Figure 19: Selected MCMC trace plots for **(i)** log of blood glucose concentration at time t=1 (g_1), **(ii)** log of blood glucose concentration at time t=288 (g_{288}), **(iii)** log of blood insulin concentration at time t=100 (i_{100}), **(iv)** log of active insulin concentration at time t=200 (x_{200}).

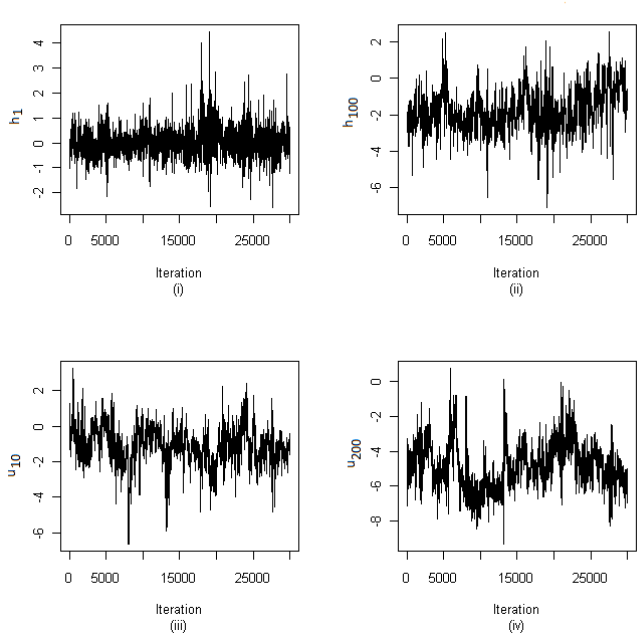

Figure 20: Selected MCMC trace plots for **(i)** log of hepatic glucose release at time t=1 (h_1), **(ii)** log of hepatic glucose release at time t=100 (h_{100}), **(iii)** log of peripheral glucose uptake at time t=10 (u_{10}), **(iv)** log of peripheral glucose uptake at time t=200 (u_{200}).

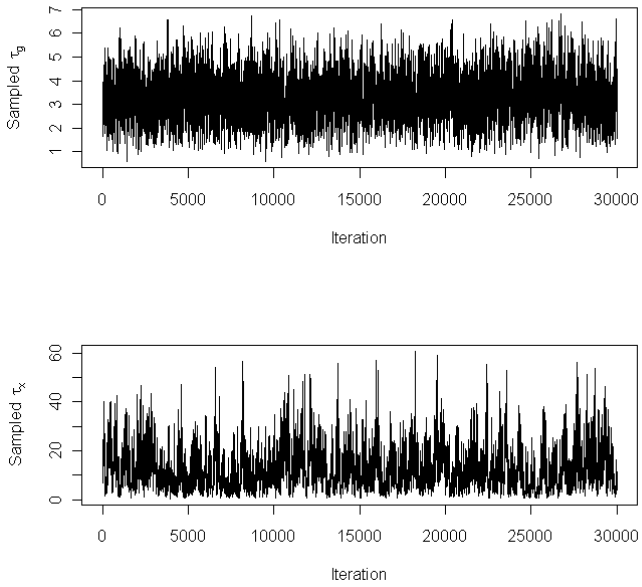

Figure 21: MCMC trace plots for τ_g (top) and τ_x (bottom).

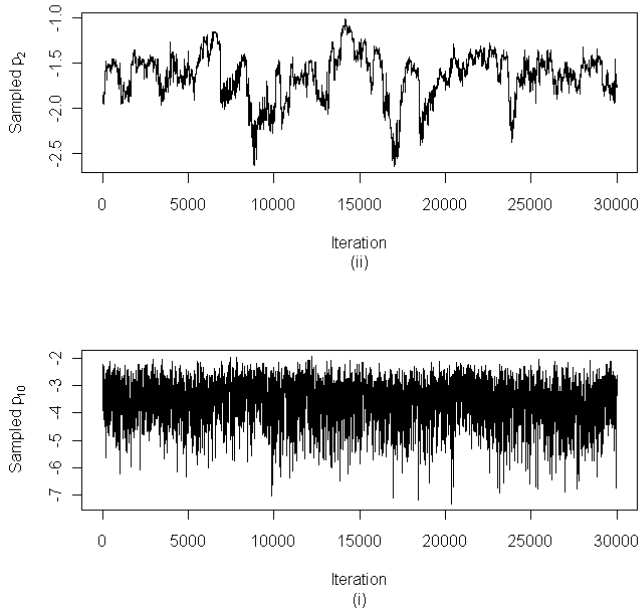

Figure 22: MCMC trace plots for p_2 (top) and p_{10} (bottom).

olate modelling assumptions. A new physiologically-based compartmental model of glucose-insulin dynamics was developed to cope with free-living data, and converted to a Bayesian network to account for process and measurement variability; MCMC methods were then proposed as a tool for model analysis.

A simulation study found that although MCMC was unable to accurately determine estimates for all parameters, it was able to produce accurate estimates for the majority of parameters. Precisions were generally overestimated, but all credible intervals contained the respective values of τ used for simulation; credible intervals of other parameters were less ideal, but with no obvious bias in most cases. MCMC performance in the predictive space was tested under a number of scenarios, including parameter misspecification and misleading informative prior distributions; variation in performance was relatively small, suggesting robustness to situations where incorrect prior information is included in the estimation procedure.

Finally, the use of our methods was demonstrated in a real-world example on an individual. Model behaviour was as anticipated with respect to profiles of the unobservable processes (plasma and active insulin, and peripheral uptake and hepatic glucose release due to activity).

Future work may investigate the potential association of parameters estimates and physical characteristics (e.g., percentage of body fat, cardiovascular fitness); such research may indicate "preferable" (in terms of long-term health outcomes) ranges of parameter values, and might further be used to assess the effect of, say, exercise intervention programmes (under the caveat of as yet unknown inter- and intra-individual variation).

Although we have not yet thoroughly tested the ability of MCMC to estimate parameters using longer chains, nor other methods (e.g. sequential Monte Carlo) that may also improve computation time, we have demonstrated a new approach to analysis of mathematical models in diabetes research. We believe an individualised, stochastic representation of blood glucose is more physiologically realistic compared to generic, deterministic models; hence, we believe the methods presented in this article are an important step towards realising the goal of an artificial pancreas.

Appendix

The equations of the exercise model, as described by Roy and Parker,[2] are given in this section, and parameter estimates are presented in Table 6.

The physical activity (E) input is modelled to account for the delay be-

tween activity onset and physiological response:

$$\dot{E}(t) = -a_1 E(t) + a_2 M_E(t),$$

where M_E is measured activity intensity above basal level. Physical activity affects insulin clearance (Z; μU/ml/min), hepatic glucose release (H; mg/kg/min) and peripheral glucose uptake (U; mg/kg/min):

$$\begin{aligned}\dot{Z}(t) &= a_3 E(t) - a_4 Z(t)\\ \dot{H}(t) &= a_5 E(t) - a_6 H(t)\\ \dot{U}(t) &= a_7 E(t) - a_8 U(t).\end{aligned}$$

Glycogenolysis, the dominant form of glucose production in the liver, slows when glycogen reserves are depleted during prolonged or intense exercise; this results in a decrease in hepatric glucose release. The dynamics of glycogenolysis are modelled by:

$$\dot{K}(t) = \begin{cases} 0 & \text{if } A(t) < A_{\text{TH}} \\ a_9 & \text{if } A(t) \geq A_{\text{TH}} \\ -K(t)/a_{10} & \text{if } M_E(t) = 0, \end{cases}$$

where A_{TH} is a threshold (based on a linear function of activity intensity) above which hepatic glucose release begins to decline, and A(t) is integrated exercise intensity:

$$\dot{A}(t) = \begin{cases} M_E(t) & \text{if } M_E(t) > 0 \\ A(t)/a_{11} & \text{if } M_E(t) = 0. \end{cases}$$

Blood insulin concentration (I; μU/ml) is modelled by

$$\frac{dI(t)}{d\text{t}} = \dot{I}(t) = -a_{12} I(t) + a_{13} U_I(t) - Z(t),$$

where a_{12} is insulin clearance, a_{13} is the inverse of insulin distribution space, and U_I is insulin infusion rate. Active insulin (X; min^{-1}) is modelled by

$$\dot{X}(t) = -a_{14} X(t) + a_{15}[I(t) - a_{16}],$$

where a_{14} is the rate of insulin degradation, a_{15} is the rate of appearance of insulin in the active compartment, and a_{16} is basal plasma insulin concentration.

Blood glucose concentration (G; mg/dl) is modelled by:

$$\begin{aligned}\dot{G}(t) = &- a_{17}(G(t) - a_{18}) - X(t)G(t) \\ &+ (W/V_G)[H(t) - K(t) - U(t)] + U_G(t)/V_G,\end{aligned}$$

where a_{17} is insulin-independent glucose metabolism, a_{18} is basal BGC, W is the individual's weight, U_G is rate of glucose absorption after meals, and V_G is glucose distribution space.

Table 6: Parameter values as presented by Roy and Parker (RP).[2]

Parameter	**RP estimate**	**Parameter**	**RP estimate**
a_1	0.8	a_{10}	6
a_2	0.8	a_{11}	0.001
a_3	0.00125	a_{12}	0.142
a_4	0.075	a_{13}	0.098
a_5	0.00158	a_{14}	0.05
a_6	0.056	a_{15}	0.000028
a_7	0.00195	a_{16}	
a_8	0.0485	a_{17}	0.035
a_9	0.0108	a_{18}	80

Acknowledgments

References

1. DCCT Research Group. The effect of intensive treatment of diabetes on the development and progression of long-term complications in insulin-dependent diabetes mellitus. *New England Journal of Medicine*, 329(14):977–986, 1993.

2. A. Roy and R. S. Parker. Dynamic modeling of exercise effects on plasma glucose and insulin levels. *Journal of Diabetes Science and Technology*, 1(3):338–347, 2007.

3. M. Hernandez-Ordonez and D. U. Campos-Delgado. An extension to the compartmental model of type 1 diabetic patients to reproduce exercise periods with glycogen depletion and replenishment. *Journal of Biomechanics*, 41:744–752, 2008.

4. M. D. Breton. Physical activity - the major unaccounted impediment to closed loop control. *Journal of Diabetes Science and Technology*, 2:169–174, 2008.

5. D. Elleri, D. B. Dunger, and R. Hovorka. Closed-loop insulin delivery for treatment of type 1 diabetes. *BMC Medicine*, 9, 2011.

6. J. J. Valletta. Dynamic modelling of the effect of physical activity on capillary blood glucose concentration in people with type 1 diabetes. PhD Thesis, 2011.

7. DCCT/EDIC Study Research Group. Intensive diabetes treatment and cardiovascular disease in patients with type 1 diabetes. *New England Journal of Medicine*, 353(25):2643–2653, 2005.

8. S. S. Soedamah-Muthu, J. H. Fuller, H. E. Mulnier, V. S. Raleigh, R. A. Lawrenson, and H. M. Colhoun. All-cause mortality rates in patients with type 1 diabetes mellitus compared with a non-diabetic population from the UK general practice research database, 1992-1999. *Diabetologia*, 49:660–666, 2006.

9. G. Marchetti, M. Barolo, L. Jovanovic, H. Zisser, and D. E. Seborg. A feedforward-feedback glucose control strategy for type 1 diabetes mellitus. *Journal of Process Control*, 18:149–162, 2008.

10. P. Soru, G De Nicolao, C. Toffanin, C. Dalla Man, C. Cobelli, and L. Magni. MPC based artificial pancreas: Strategies for individualization and meal compensation. *Annual Reviews in Control*, 36:118–128, 2012.

11. A. Abu-Rimleh and W. Garcia-Gabin. Feedforward-feedback multiple predictive controllers for glucose regulation in type 1 diabetes. *Computer Methods and Programs in Biomedicine*, 99(1):113–123, 2010.

12. G. Quiroz and R. Femat. Theoretical blood glucose control in hyper- and hypoglycemic and exercise scenarios by means of an H_∞ algorithm. *Journal of Theoretical Biology*, 263:154–160, 2010.

13. R. Hovorka, K. Kumareswaran, J. Harris, J. M. Allen, D. Elleri, D. Xing, C. Kollman, M. Nodale, H. R. Murphy, D. B. Dunger, S. A. Amiel, S. R. Heller, M. E. Wilinska, and M. L. Evans. Overnight closed loop insulin delivery (artificial pancreas) in adults with type 1 diabetes: crossover randomised controlled studies. *British Medical Journal*, 342, 2011.

14. D. A. Gough, K. Kreutz-Delgado, and T. M. Bremer. Frequency characterization of blood glucose dynamics. *Annals of Biomedical Engineering*, 31:91–97, 2003.

15. B. E. Ainsworth, W. L. Haskell, M. C. Whitt, M. L. Irwin, A. M. Swartz, S. J. Strath, W. L. O'Brien, Bassett Jnr. D. R., K. H. Schmitz, P. O. Emplaincourt, D. R. Jacobs Jnr., and A. S. Leon. Compendium of physical activities: an update of activity codes and MET intensities. *Medicine & Science in Sports & Exercise*, 32:S498S504, 2000.

16. E. D. Lehmann and T. Deutsch. A physiological model of glucose-insulin interaction in type 1 diabetes mellitus. *Journal of Biomedical Engineering*, 14:235–242, 1992.

17. C. Tarin, E. Teufel, J. Pic, J. Bondia, and H.-J. Pfleiderer. Comprehensive pharmacokinetic model of insulin glargine and other insulin formulations. *IEEE Transactions on Biomedical Engineering*, 52(12):1994–2005, 2005.

18. R. N. Bergman, Y. Z. Ider, C. R. Bowden, and C. Cobelli. Quantitative estimation of insulin sensitivity. *American Physiological Society*, 236(6):667–677, 1979.

19. R. N. Bergman, L. S. Phillips, and C. Cobelli. Physiologic evaluation of factors controlling glucose tolerance in man. *Journal of Clinical Investigation*, 68(6):1456–1467, 1981.

20. B. Zajadacz, A. Skarpańska-Stejnborn, W. Brzenczek-Owczarzak, A. Juszkiewicz, M. Naczk, and Z. Adach. The influence of physical exercise on alterations in concentrations of neuropeptide Y, leptin and other selected hormonal and metabolic parameters in sportspeople. *Biology of Sport*, 26:309–324, 2009.

21. K. F. Petersen, T. B. Price, and R. Bergeron. Regulation of net hepatic glycogenolysis and gluconeogenesis during exercise: Impact of type 1 diabetes. *The Journal of Clinical Endocrinology & Metabolism*, 89:46564664, 2005.

22. T. Arleth, S. Andreassen, M. O. Federici, and M. M. Benedetti. A model of the endogenous glucose balance incorporating the characteristics of glucose transporters. *Computer Methods and Programs in Biomedicine*, 62:219–234, 2000.

23. K. E. Andersen and M. Højbjerre. A population-based Bayesian approach to the minimal model of glucose and insulin homeostasis. *Statistics in Medicine*, 24:2381–2400, 2005.

24. R. Durrett. *Probability: Theory and Examples*. Cambridge University Press, fourth edition, 2010.

25. W. R. Gilks, S. Richardson, and D. J. Spiegelhalter. *Markov Chain Monte Carlo in Practice*. Chapman & Hall, 1996.

26. T. Gneiting and A. E. Raftery. Strictly proper scoring rules, prediction, and estimation. *Journal of the American Statistical Association*, 102:359–378, 2007.